Chemical Science

ROYAL SOCIETY OF CHEMISTRY

EDGE ARTICLE

View Article Online
View Journal | View Issue

Cite this: *Chem. Sci.*, 2025, **16**, 14286

All publication charges for this article have been paid for by the Royal Society of Chemistry

Received 31st March 2025
Accepted 23rd June 2025

DOI: 10.1039/d5sc02436f

rsc.li/chemical-science

A general transition metal binding aptamer following the Irving–Williams series†

Jin Wang,[ab] Yunus A. Kaiyum,[c] Sihan Wang,[b] Xiangmei Li,[a] Hongtao Lei,[a] Philip E. Johnson[c] and Juewen Liu*[b]

Using both Co^{2+} and Ni^{2+} as target metal ions, aptamer selections were carried out by immobilization of a DNA library *via* hybridization. A set of aptamers were obtained although they all showed binding to both metal ions. The Co-1 aptamer was highly enriched in both selections and it is a general metal binding aptamer with binding affinity following the Irving–Williams series: $Mn^{2+} < Fe^{2+} < Co^{2+} < Ni^{2+} < Cu^{2+} > Zn^{2+}$. Using NMR spectroscopy, Co-1 forms new base pairs with a relatively large structural change upon binding to Zn^{2+}, whereas a previously reported Zn-1 aptamer shows less conformational change and rigidifies upon Zn^{2+} binding. The induced-fitting of the Co-1 aptamer and the lock-and-key binding of the Zn-1 aptamer may explain the general metal binding of the former. Using isothermal titration calorimetry, Co-1 binding Co^{2+} was an enthalpy-driven event and the K_d was determined to be 2.7 μM, whereas the K_d from the strand-displacement assay was 76 nM. The Co-1 aptamer is the first reported aptamer to follow the Irving–Williams series, although this series is very prevalent in proteins. This aptamer can thus serve as a model system for understanding metal binding by DNA and can also be a general first-row transition metal sensing element.

Introduction

The first-row transition metal ions are particularly important in biology and many of them are essential cofactors in metalloenzymes.[1] In most metalloproteins, the affinity of metal binding follows the Irving–Williams series: $Mn^{2+} < Fe^{2+} < Co^{2+} < Ni^{2+} < Cu^{2+} > Zn^{2+}$.[2] This high affinity for copper has led to the so-called "copper tyranny", and organisms have to employ complex non-equilibrium strategies to keep other metal ions in their binding sites.[3]

Studies in metal binding sites in nucleic acids never seemed to have encountered this "copper tyranny" problem. In the early days, metal binding studies were performed in ribozymes and later in DNAzymes, since they in general require divalent metal ions as cofactors to achieve catalytic activities.[4–8] Later, different metal ions were intentionally used to select for DNAzymes that can achieve metal-specific activities, which are useful as biosensors for metal detection.[9–12] Cu^{2+} is probably one of the poorest metal ions in promoting the RNA cleavage reaction,[13] although in some modified DNAzymes, it showed a high activity.[14] DNAzymes specific for Mn^{2+},[15] Fe^{2+}/Fe^{3+},[11] Ni^{2+},[16] Cu^{2+},[17] and Zn^{2+} ions[18,19] have been reported, although some contained chemical modifications in DNAzymes to achieve the needed specificity and activity. The activity of many ribozymes was found to correlate with affinity to phosphate instead of following the Irving–Williams series.[8] These metal ions, however, do not need to stably bind to ribozymes or DNAzymes to exert their catalytic activities. They only need to transiently bind to the transition state and neutralize the negative charges in the scissile phosphate in most cases.[7,13,20]

To study metal binding sites in DNA, aptamers are more relevant. Aptamers are single-stranded nucleic acids that can selectively bind to target molecules.[4,21,22] The isolation of metal-specific aptamers has been carried out for a long time with early examples in the 1990s. Back then, the selection was achieved by the immobilization of metal ions such as Ni^{2+} and Zn^{2+} on a chelation bead and the focus was on RNA aptamer selection.[23,24] Such aptamers were rarely used for applications due to the poor stability of RNA. Later, aptamer selection by immobilization of a DNA library (so called capture-SELEX) had been developed, which allows the use of free metal ions as targets.[25,26] Ellington's group first used this method to isolate an aptamer for Zn^{2+}, although this aptamer contained a fluorophore.[27] Soh and coworkers used an interesting strategy to isolate aptamers for Cu^{2+} and Hg^{2+}.[28] Jahan *et al.* aimed to select aptamers for the PD-L1 protein by immobilizing the PD-L1 protein on nickel nitrilotriacetic acid (Ni–NTA) beads. Interestingly, due to the presence of Ni^{2+} on the beads, the selected aptamer showed binding to Ni^{2+} instead of the PD-L1 protein.[29] Capture-SELEX has also been used to obtain aptamers for many transition metal ions including Cd^{2+},[30] Pb^{2+},[31] Zn^{2+},[32] and Cu^{2+}.[33] In each case, the aptamers were

[a]*Guangdong Provincial Key Laboratory of Food Quality and Safety, College of Food Science, South China Agricultural University, Guangzhou 510642, China*

[b]*Department of Chemistry, Waterloo Institute for Nanotechnology, University of Waterloo, Waterloo, Ontario N2L 3G1, Canada. E-mail: liujw@uwaterloo.ca*

[c]*Department of Chemistry, York University, 4700 Keele Street, Toronto, Ontario M3J 1P3, Canada*

† Electronic supplementary information (ESI) available. See DOI: https://doi.org/10.1039/d5sc02436f

able to bind to their target metal ion with the highest affinity. So far, Irving–Williams series was only seen in a duplex thermal stability assay using DNA containing imidazole-derived nucleobases.[34] Thus, it seems that the Irving–Williams series has yet to be observed in unmodified nucleic acids.

Thus, an interesting question is whether nucleic acids are capable of binding metal ions following the Irving–Williams series. The chemical diversity for interacting with metal ligands in nucleic acids is much less compared to that in proteins.[35] For example, nucleic acids lack thiol ligands that have strong affinity with copper. Co^{2+} and Ni^{2+} are interesting metal ions and they differ from Cu^{2+} and Zn^{2+} by having slower ligand exchange rates.[36] In this study, we performed two capture-SELEX experiments using Co^{2+} and Ni^{2+} as target metal ions. Interestingly, the most abundant aptamers followed the Irving–Williams series, with Cu^{2+} binding being much stronger than that for Co^{2+} or Ni^{2+}. Yet, such a sequence was not observed during our previous Cu^{2+} selection.[33] By using NMR and isothermal titration calorimetry (ITC), we attempted to further compare this general metal aptamer to some specific aptamers to gain fundamental insights.

Materials and methods

Chemicals and DNA are described in the ESI.†

SELEX

A library-immobilized selection strategy was employed as previously described.[33,37] $CoCl_2 \cdot 6H_2O$ and $NiCl_2 \cdot 6H_2O$ were dissolved in 100 mM Milli-Q water, and diluted with SELEX buffer for selection. For Co^{2+} selection, the concentrations were set at 10 μM for rounds 1–14 and reduced to 2 μM for rounds 15–17. Similarly, for Ni^{2+} selection, 10 μM was used for rounds 1–13, followed by 2 μM for rounds 14–17. The last round's PCR products were sequenced at the McMaster University Genome Facility, and the sequencing results were analyzed using Geneious Prime software (Auckland, New Zealand).

Thioflavin T (ThT)-based binding assay

The fluorescence spectra of the ThT-based assay were measured using a Varian Eclipse fluorescence spectrophotometer (CA, USA). The assay contained 0.5 μM aptamer and 1 μM ThT in 500 μL of selection buffer. The mixture was transferred to a quartz cuvette. Metal ions were added or titrated until equilibrium was reached. Fluorescence was excited at 440 nm, and the emission spectra were recorded between 460 and 520 nm. Fluorescence at 490 nm served as the basis for calculations. The initial fluorescence of the aptamer/ThT mixture is denoted as F_0, and the value after metal ion addition is F. The ratio F/F_0 was plotted, and the K_d was determined using the equation $y = y_0 + aK_d/(K_d + [M^{2+}])$, where a represents the maximal fluorescence signal change at saturation.

Fluorescence strand-displacement assay

Fluorescence strand-displacement assays were performed using a Tecan Spark F200 microplate reader (Switzerland) in a 96-well microplate. The excitation and emission wavelengths were set at 485 nm and 520 nm, respectively. To prepare the displacement sensor, 1 μL of FAM-labeled Co-1 aptamer (100 μM), 2 μL of quencher-cDNA (100 μM), and 97 μL of SELEX buffer were mixed, annealed at 85 °C for 1 min, and gradually cooled to room temperature for 30 min, followed by cooling at 4 °C for 30 min and then at −20 °C for 30 min. For the test, 2 μL of annealed aptamer was added to 98 μL SELEX buffer, and baseline fluorescence was recorded for 5 min. Subsequently, 2 μL of Co^{2+} or other metal ions at different concentrations were introduced, and fluorescence was monitored for another 10 min. Fluorescence changes were calculated using the formula $(F - F_0)/F_0$, where F_0 represents the initial fluorescence before metal ion addition and F corresponds to the fluorescence after adding metal ions.

NMR

NMR experiments on the DNA aptamer sample were performed using a 600 MHz Bruker Avance spectrometer. All NMR spectra were acquired with an aptamer concentration of 0.5 mM in an aqueous solution with 100 mM NaCl and 2 mM $MgCl_2$ in 10% D_2O at 5 °C. Water suppression was achieved using excitation sculpting.[38]

Circular dichroism (CD) spectroscopy

CD spectra were recorded using a Chirascan spectropolarimeter (Applied Photophysics Ltd, Surrey, UK) with procedures reported in previous experiments.[39] Aptamers (5 μM) were prepared in 10 mM MES buffer (pH 6.0) containing 100 mM NaCl and 2 mM $MgCl_2$. Measurements were conducted before and after adding 20 μM metal ions. The wavelength range was from 230 to 320 nm with a bandwidth of 4 nm, and a 1 cm path-length cuvette was used.

ITC

Isothermal titration calorimetry (ITC) was conducted with a MicroCal iTC200 instrument (Worcestershire, UK) to test binding by the Co-1 aptamer. The aptamer (20 μM) in the SELEX buffer was annealed by heating to 95 °C for 5 min and cooling naturally over 30 min. Subsequently, both the aptamer and ions (333 μM in the SELEX buffer) were degassed for 5 min before loading. Then, 300 μL of the aptamer was loaded into a cell chamber and a syringe was filled with 75 μL of metronidazole. After an initial injection of 0.5 μL, subsequent injections of the target were titrated into the cell at a rate of 2.0 μL per injection over a duration of 5.0 seconds, totaling 20 injections at 25 °C. Each titration was spaced 240 seconds apart. The binding constant was determined by fitting the titration curve to a one-site binding model using Origin software.

Results and discussion

Selection of DNA aptamers for Co^{2+} and Ni^{2+}

The selection of DNA aptamers for Co^{2+} and Ni^{2+} was carried out using a library containing a 30-nucleotide (nt) random region as described previously (Table S1†).[33] This library was immobilized

on streptavidin-coated beads *via* hybridization to a fixed PCR primer binding region. After adding target metal ions, some aptamer sequences may bind the metal ions and be released from the beads for PCR amplification. Since we aimed to achieve high affinity aptamers for Co^{2+} and Ni^{2+}, a low target metal ion concentration of 10 μM was used in the initial rounds.[40–42] In the final three or four rounds, the metal ion concentration was further decreased to 2 μM (see Table S2† for the selection conditions). The round 17 libraries were deep sequenced and the sequences were highly converged suggesting successful selections.

Fig. 1A shows the alignment of the top 10 most abundant Co^{2+} sequences. The predominant sequence in the Co^{2+} selection named Co-1 has an abundance of 10.3% and its mFold predicted secondary structure is shown in Fig. 1B. Co-1 is predicted to fold into a three-way junction linked by a few nucleotides, and these linking nucleotides (in red) are highly conserved. Therefore, it is likely that Co^{2+} binding takes place in the middle pocket formed by the linking nucleotides.

For the Ni^{2+} sequencing results (Fig. 1C), the Ni-3 sequence is identical to that of Co-1, suggesting that this sequence can bind to both metals. Ni-1 is a representative sequence of another family. We also folded Ni-1 as shown in Fig. 1D. Based on the family assignment, Co-1 (same as Ni-3), Co-2, Ni-1, and Ni-4 were selected for further testing. The alignment of the top 20 sequences from Co^{2+} and Ni^{2+} selections is presented in Fig. S1 and S2.†

Aptamer binding to Co^{2+} and Ni^{2+} using ThT fluorescence spectroscopy

We first used Thioflavin T (ThT) fluorescence spectroscopy as a rapid assay to evaluate binding of these selected aptamers. ThT, as a free dye, exhibits almost no fluorescence. It can bind to any DNA, including aptamers, leading to fluorescence enhancement. When a DNA aptamer binds to its target, ThT is displaced, resulting in a fluorescence decrease.[26,43] The ThT assay has been successfully applied to study aptamer binding to rare earth ions,[37] Cu^{2+},[33] and other targets.[26,32] We first collected the fluorescence spectra of the Co-1 aptamer/ThT mixture with increasing concentrations of Co^{2+} and Ni^{2+}. Both metal ions induced over a 50% fluorescence drop at 2 μM metal concentration (Fig. 2A and C). Based on the titration results, the Co-1 aptamer has a K_d of 731 nM for Co^{2+} and 467 nM for Ni^{2+} (Fig. 2B and D). Ni-4 exhibited a K_d of 901 nM for Co^{2+} and 257 nM for Ni^{2+} in the same titration (Fig. S3†). The Co-2 and Ni-1 aptamers, in contrast, required higher Co^{2+} and Ni^{2+} concentrations to show a fluorescence decrease (Fig. S4†). Thus, Co-1 and Ni-4 are higher affinity aptamers. Although the

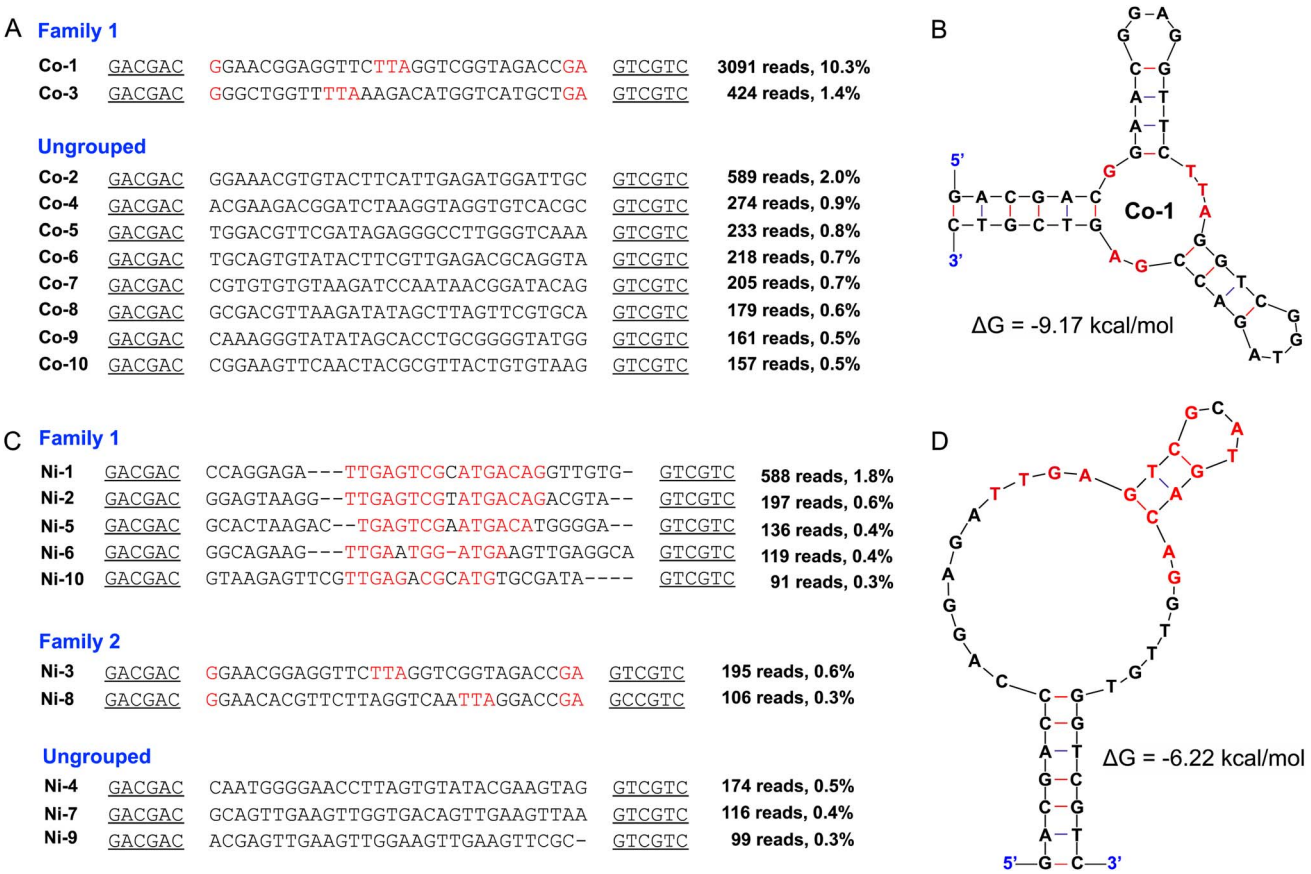

Fig. 1 Alignment of the top 10 sequences for (A) the Co^{2+} selection and (C) the Ni^{2+} selection. The nucleotides in the primer-binding regions are underlined, and the conserved nucleotides are marked in red or blue. The mFold predicted secondary structure of (B) Co-1 ($\Delta G = -9.17$ kcal mol^{-1}) and (D) Ni-1 ($\Delta G = -6.22$ kcal mol^{-1}) aptamers at 25 °C, 100 mM Na^+ and 2 mM Mg^{2+}.

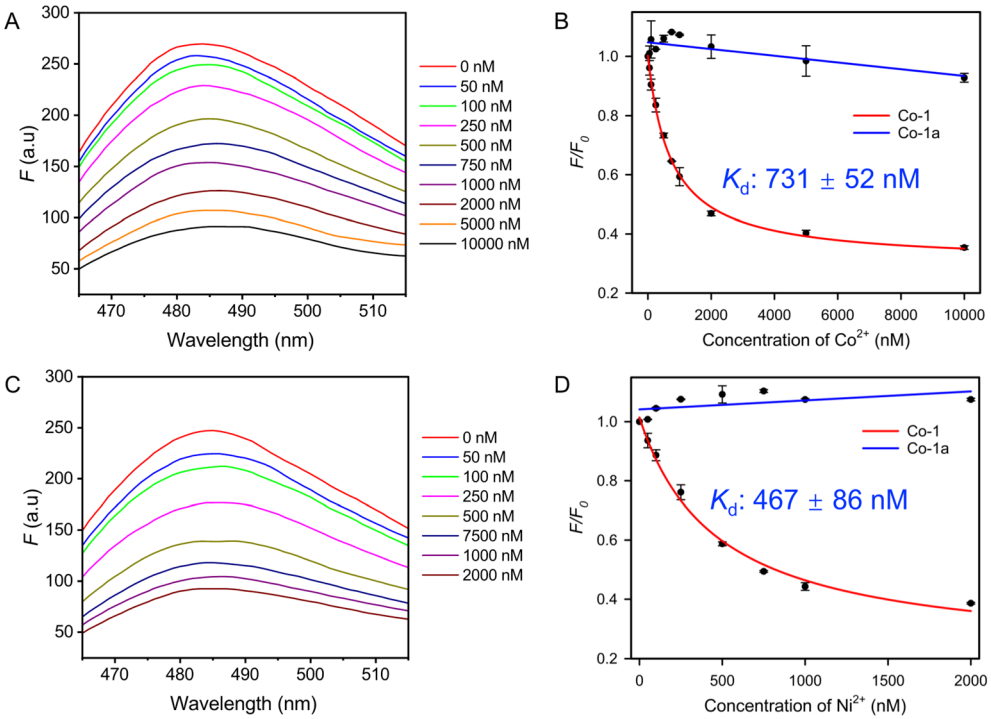

Fig. 2 The fluorescence spectra of the ThT/Co-1 mixture in the presence of different concentrations of (A) Co^{2+} and (C) Ni^{2+} in the SELEX buffer. Titration curves of (B) Cu^{2+} and (D) Ni^{2+} into the Co-1 aptamer and a nonbinding mutant Co-1a (ThT: 0.5 μM, ThT: 1 μM).

binding affinities of the two were comparable, Co-1 demonstrated the highest enrichment, and it was found in both Co^{2+} and Ni^{2+} selections. Therefore, Co-1 was chosen for further studies. As a control, a mutant named Co-1a was designed by swapping the positions of the conserved nucleotides in the loops (Fig. S5†). Titration experiments with Co^{2+} and Ni^{2+} revealed no significant fluorescence decrease (Fig. 2B and D, blue lines) for Co-1a, indicating that Co-1 exhibits specific binding for Co^{2+} and Ni^{2+}.

DNA strand-displacement binding assays

While ThT fluorescence provides a cost-effective assay for screening a large number of sequences, it is a signal-off assay and suffers from nonspecific fluorescence quenching by metal ions. Thus, we further used the strand-displacement assay (Fig. 3A).[44] The Co-1 aptamer was extended on the 5′ end by five nucleotides and it was hybridized to a 12-mer quencher-labeled cDNA (Table S1†). This hybridization complex has quenched fluorescence. In the presence of a target metal ion, the binding of the aptamer can release the quencher-labeled strand, resulting in a fluorescence increase.[37,44–46] Using this assay, we tested Co^{2+} (Fig. 3B) and Ni^{2+} (Fig. S6C†) by following the kinetics of the sensor response at different metal concentrations. For both metals, a modest fluorescence increase occurred at a metal concentration of 100 nM and a rapid fluorescence increase to the saturated value was achieved with 10 μM of the metals. Indeed, these two metal ions responded very similarly to this sensor.

We then performed careful titrations for these metal ions. The titration curve for Co^{2+} is shown in Fig. 3C and the rest are shown in Fig. S6 and S7.† The observed K_d values using the strand displacement assay are apparent K_d due to the presence of the quencher-labeled strand acting as a competitor.[47–49] The apparent K_d values were determined to be 178 μM for Mn^{2+}, 7.8 μM for Fe^{2+}, 1260 nM for Co^{2+}, 607 nM for Ni^{2+}, 139 nM for Cu^{2+}, 5.9 μM for Zn^{2+}, and 4.9 μM for Cd^{2+}. We then titrated the quencher-labeled strand with the FAM-aptamer strand to calculate the true K_d of the aptamer (see Fig. S8† for details). The corresponding true K_d values were 10 680 nM for Mn^{2+}, 468 nM for Fe^{2+}, 76 nM for Co^{2+}, 37 nM for Ni^{2+}, 8 nM for Cu^{2+}, 352 nM for Zn^{2+}, and 295 nM for Cd^{2+}.

The Co-1 aptamer follows the Irving–Williams series

In 1953, H. Irving and R. J. P. Williams proposed the Irving–Williams series, which describes the binding strength of ligands with divalent 3d transition metal ions. The binding strength increases with the atomic number of the metal, following the trend $Mn^{2+} < Fe^{2+} < Co^{2+} < Ni^{2+} < Cu^{2+} > Zn^{2+}$.[2] Fig. 4A plots the true K_d of these metal ions as a function of their positions in the periodic table from Mn^{2+} to Zn^{2+}, and it matches perfectly with this series. Thus, we have obtained the first DNA aptamer that follows the Irving–Williams series. The Irving–Williams series can be explained as follows: from Mn^{2+} to Ni^{2+}, the decreasing ionic radius leads to higher charge density, resulting in increased complex stability. Although Cu^{2+} has a slightly larger radius than Ni^{2+}, the Jahn–Teller effect provides additional stabilization for its octahedral complexes.

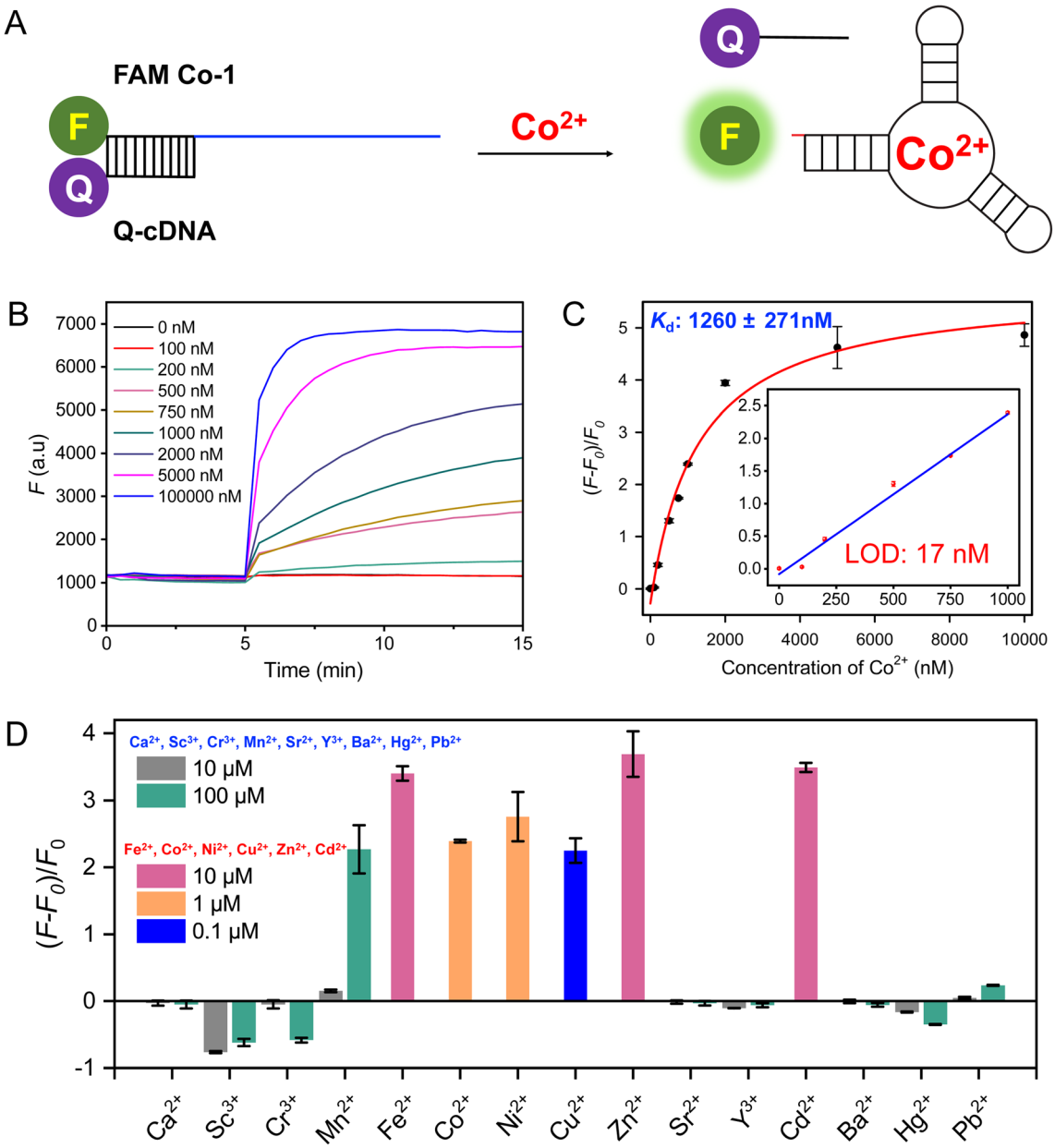

Fig. 3 (A) Scheme of the strand displacement assay for the detection of Co^{2+}. (B) Calibration curves of the sensor for Co^{2+}. (C) Kinetics traces of the FAM Co-1 sensor in the presence of various concentrations of Co^{2+} in SELEX buffer. Inset: the linear response at 1000 nM. (D) The response of Co-1 to various metal ions. After confirming the response range of Co-1 to Co^{2+} and Ni^{2+}, we further tested the response of Co-1 to other metal ions. Co^{2+} and Ni^{2+} produced significant fluorescence enhancement even at 1 μM, whereas Cu^{2+} induced a noticeable increase at as low as 0.1 μM. In contrast, Fe^{2+}, Zn^{2+}, and Cd^{2+} showed a pronounced fluorescence increase at 10 μM. At concentrations of 10 μM and even 100 μM, a significant increase in fluorescence was observed with Mn^{2+}, while no noticeable changes were detected with Ca^{2+}, Sc^{3+}, Cr^{3+}, Sr^{2+}, Y^{3+}, Ba^{2+}, Hg^{2+}, and Pb^{2+}. Therefore, this aptamer Co-1 has binding to first-row transition metal ions along with Cd^{2+}.

In contrast, Zn^{2+} has a similar radius to Cu^{2+} but possesses a filled d^{10} configuration, which limits effective orbital overlap with ligands and leads to lower complex stability.

Metal binding studies using NMR

To investigate the possible conformational changes taking place in the DNA aptamer with a ligand, we then performed ^{1}H-NMR titrations monitoring the imino region (Fig. 5).[50] For this purpose, we chose to use Zn^{2+} as Zn^{2+} is not paramagnetic and we also have previously reported a Zn^{2+} aptamer that is specific for Zn^{2+} (no binding to Co^{2+} or Ni^{2+}).[32] Based on the NMR results, the free Co-1 aptamer has approximately 9 imino proton resonances attributable to base pairs involving G and T nucleotides, approximately 6 of which are from Watson–Crick pairs located between 12 and 14 ppm. Approximately 3 are from non-Watson–Crick pairs located between 10 and 11 ppm (Fig. 5A). By examining the mFold predicted secondary structure of Co-1, 14 Watson–Crick base pairs were predicted to form. Therefore, not all these predicted base pairs were stably formed in the absence

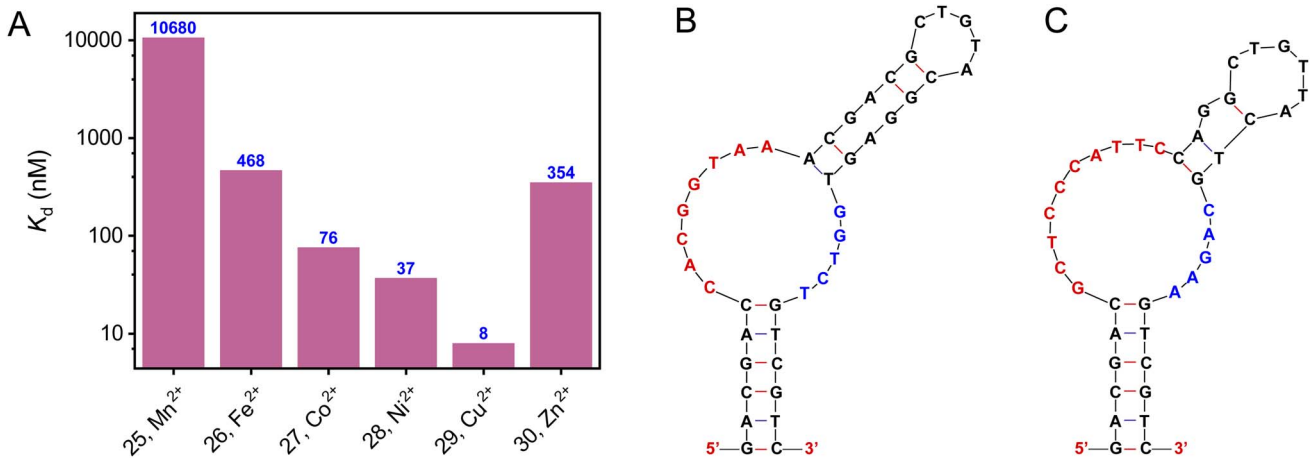

Fig. 4 (A) The relationship between the K_d of Co-1 for first-row divalent transition metals and their (A) atomic numbers and (B) radii. The predicted secondary structures and sequences of the (B) Cu-1[33] and (C) Zn-1 aptamers.[32] The conserved nucleotides on both sides of the loop region are marked in red or blue.

of Zn^{2+}. When Zn^{2+} was titrated, more peaks emerged in both regions, and a total of about 17–18 base pairs were formed. Thus, additional Watson–Crick and non-Watson–Crick pairs form upon binding to Zn^{2+} indicating that this aptamer undergoes metal-induced folding.[51] Assuming that the binding site in Co-1 is at the same location for all metal ions, the binding of Co^{2+} and Ni^{2+} should behave similarly and result in metal-induced structure formation.

For comparison, we also performed NMR on the Zn-1 aptamer (Fig. 5B). Overall, as the number of peaks observed in the imino region remained similar before and after adding Zn^{2+} the amount of structural change upon Zn^{2+} binding is less for the Zn-1 aptamer. Due to the sharpening of the imino signals this aptamer may have a pre-formed binding pocket that is stabilized upon binding to Zn^{2+}. This aptamer might have a higher metal binding selectivity due to this hypothesised pre-

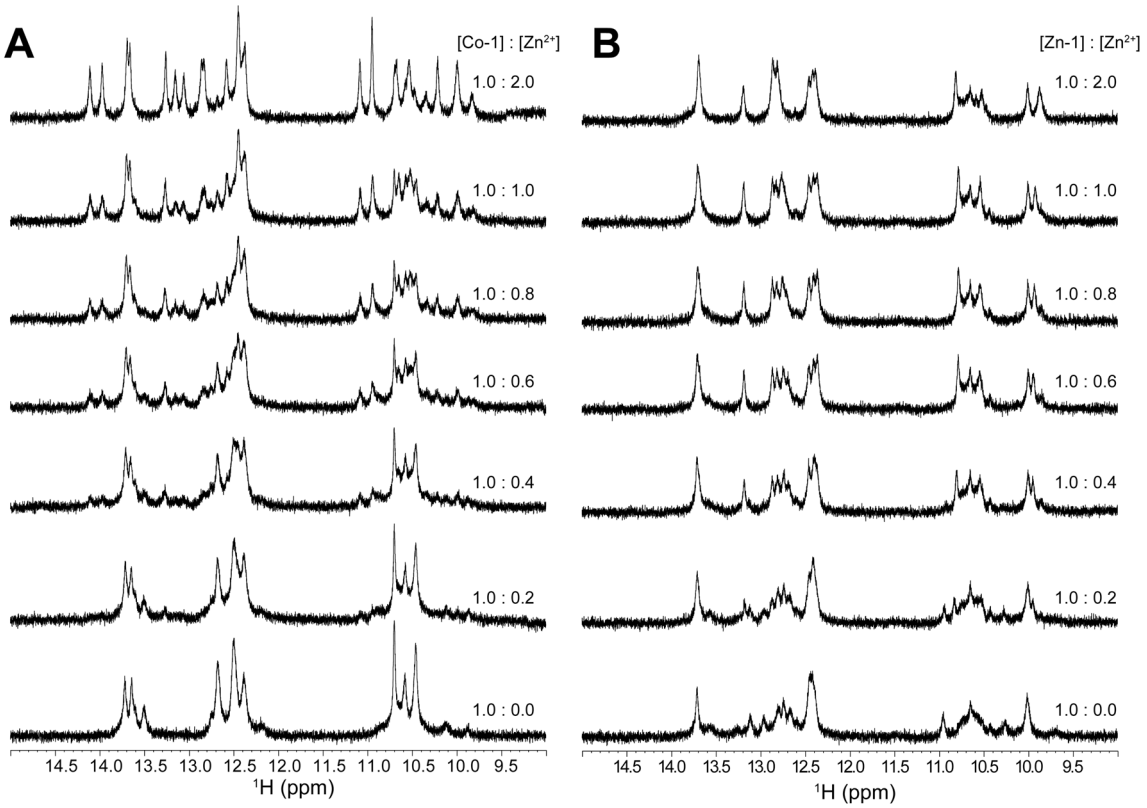

Fig. 5 1D ^{1}H-NMR of the imino proton region of the (A) Co-1 and (B) Zn-1 aptamers binding Zn^{2+} ions. Data were acquired at 5 °C in 100 mM NaCl, 2 mM $MgCl_2$, 10% D_2O.

formed binding pocket. Without high resolution structures, this hypothesis is speculative.

Metal binding studies using CD spectroscopy

CD spectroscopy reflects the differential absorption of left and right circularly polarized light, and it can provide information regarding the secondary structure of aptamers.[52,53] The Co-1 aptamer exhibited a characteristic positive peak at 278 nm and a negative peak at 244 nm (Fig. S9†). The positive peak is attributed to base stacking, while the negative peak indicates the helicity of the polynucleotide chain.[54,55] Upon the addition of 20 μM transition metal ions, the intensity of the positive peak decreased significantly, while the negative peak also reduced slightly. Mn^{2+} did not cause much spectral change attributable to its low affinity to this aptamer. This result suggests that transition metal ions binding induced a substantial conformational rearrangement in the Co-1 aptamer, likely leading to partial disruption or reorganization of the base stacking. This observation is consistent with our NMR results, which showed the appearance of new imino proton resonances upon Zn^{2+} titration, indicating the formation of additional Watson–Crick and non-canonical base pairs and the overall folding of the aptamer into a more structured conformation. However, such Zn^{2+}-induced folding appears to involve non-B-form structural motifs, resulting in a less regular base stacking pattern and hence a reduced CD signal at 278 nm.

In contrast, the Zn-1 aptamer displayed spectral changes in an opposite way upon Zn^{2+} addition, with a slight increase in the intensity of the positive CD band at 278 nm (Fig. S10†), suggesting that the aptamer adopts a well-folded structure even in the absence of metal ions. The modest enhancement in base stacking upon Zn^{2+} binding indicates that the Zn-1 aptamer possesses a pre-organized binding pocket that is further stabilized by the metal ion. This interpretation is supported by the NMR results, where no significant changes were observed in the imino proton region after Zn^{2+} addition, confirming that Zn-1 undergoes only subtle conformational adjustments.

Metal binding studies using ITC

Finally, we characterized metal binding using ITC. Cu^{2+} and Zn^{2+} could not give good ITC results likely due to the hydrolysis of these metal ions in buffer. When injected into the sample chamber, the heat associated with diluting hydrolyzed metal species can dominate the signal. Therefore, we could only titrate Co^{2+} into the Co-1 aptamer (Fig. 6). A typical binding curve was observed with a ΔH of -16.4 kcal mol^{-1} and a ΔS of -29.6 cal mol^{-1} K^{-1} ($T\Delta S = -8.8$ kcal mol^{-1}). Therefore, the binding of Co-1 to Co^{2+} ions was driven by enthalpy, which compensated for the penalty due to entropy loss. The enthalpy gain could be from the formation of new base pairs seen in NMR, along with the coordination of Co^{2+}.

Selection outcomes

Since this Co-1 aptamer can bind Cu^{2+} even stronger than Co^{2+} (Fig. 4A), we then searched the library for previously reported Cu^{2+} selection.[33] For the top 1000 sequences, we did not find the

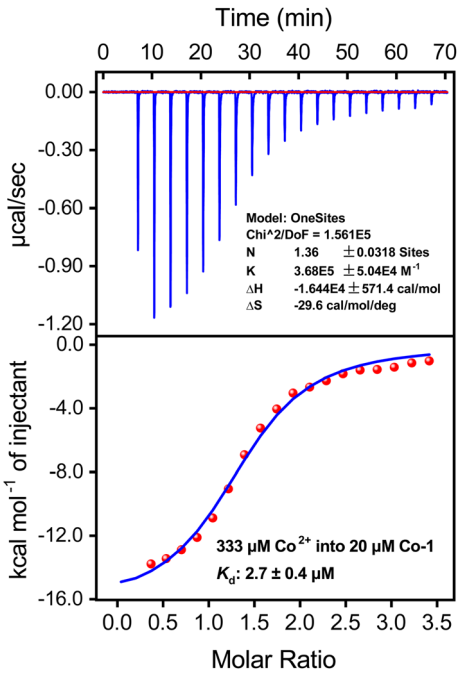

Fig. 6 Titration of 333 μM Co^{2+} into the 20 μM Co-1 aptamer.

Co-1 aptamer. It is interesting to note that when we used Zn^{2+} or Cu^{2+} for the selection, we obtained highly specific aptamers for them. However, when we used Co^{2+} and Ni^{2+}, we obtained a highly general aptamer. The secondary structures of the Cu-1 aptamer and Zn-1 aptamer are shown in Fig. 4B and C, respectively. They have quite similar secondary structures with conserved metal binding regions formed by the two loops. The Co-1 and Cu-1 aptamers have a similar affinity to Cu^{2+}. The number of conserved nucleotides is much lower in Co-1, and this may explain its lower specificity and its ability to accommodate many divalent metal ions. Co-1 may only be able to capture the information of divalent transition metals (two charges and a certain size range). In contrast, the Cu-1 and Zn-1 aptamers have a larger binding pocket allowing them to form more complex binding structures that can better fit the orbitals of the metal ions. Although metal ions are not in general considered to have shapes, they do have different coordination geometries. Such information may be captured by the more complex aptamers, likely *via* inner sphere coordination.

Based on numerous additional signals appearing in the NMR spectra of the Co-1 aptamer in the presence of Zn^{2+}, new base pairs form in this aptamer upon metal binding. In contrast, for the Zn-1 aptamer, no new imino peaks appeared indicating that a small amount of few new structure forms. Instead, the set of low intensity imino signals in the free Zn-1 aptamer gives rise to a few strong signals indicating the appearance of a more defined structure in the metal-bound Zn-1 aptamer. Therefore, we hypothesize that the Co-1 aptamer has an induced-fit mechanism, and added metal ions induced the formation of the bound structure. This binding site follows the Irving–Williams series and thus the intrinsic properties of the metal ions dominated the stability of the binding. In contrast,

the Zn-1 aptamer has a binding mechanism where the binding site rigidifies with metal binding, which may explain its better selectivity.

Conclusions

In this work, an interesting DNA aptamer named Co-1 was isolated using capture-SELEX for both Co^{2+} and Ni^{2+} as target metal ions. This is the first aptamer that shows a clear binding affinity trend following the Irving–Williams series. This series is quite common in proteins,[56] and we demonstrated here that DNA can also have comparable metal binding sites. This Co-1 aptamer will be a useful model system to study metal binding by DNA aptamers. Having aptamers that are specific for a group of metal ions is also interesting. We previously reported a DNAzyme that can recognize all trivalent lanthanides,[57] and all thiophilic metals.[20] The 17E DNAzyme can use nearly all divalent metals for catalysis.[13] This aptamer may also serve as a general first-row transition metal biosensor.

Data availability

The data that support the findings of this study are available from the the Federated Research Data Repository, at **https://doi.org/10.20383/103.01328**.

Author contributions

Jin Wang performed the aptamer selections, collected data, proposed key ideas, and drafted the initial manuscript. Yunus A. Kaiyum and Philip E. Johnson were responsible for the NMR experiments. Sihan Wang conducted the ITC experiments. Xiangmei Li and Hongtao Lei provided valuable suggestions during manuscript preparation and support for some CD experiments. Juewen Liu contributed to conceptualization, data analysis, manuscript revision, and funding acquisition. All authors discussed the results and commented on the manuscript.

Conflicts of interest

There are no conflicts to declare.

Acknowledgements

Funding for this work was from the Natural Sciences and Engineering Research Council of Canada (NSERC). Jin Wang received a China Scholarship Council (CSC, 202308440518) scholarship to visit the University of Waterloo.

References

1 Y. Lu, N. Yeung, N. Sieracki and N. M. Marshall, *Nature*, 2009, **460**, 855–862.
2 H. Irving and R. Williams, *J. Chem. Soc.*, 1953, 3192–3210.
3 D. Osman and N. J. Robinson, *FEBS Lett.*, 2023, **597**, 141–150.
4 W. Zhou, R. Saran and J. Liu, *Chem. Rev.*, 2017, **117**, 8272–8325.
5 R. J. Lake, Z. Yang, J. Zhang and Y. Lu, *Acc. Chem. Res.*, 2019, **52**, 3275–3286.
6 R. K. Sigel and A. M. Pyle, *Chem. Rev.*, 2007, **107**, 97–113.
7 W. L. Ward, K. Plakos and V. J. DeRose, *Chem. Rev.*, 2014, **114**, 4318–4342.
8 J. Schnabl and R. K. Sigel, *Curr. Opin. Chem. Biol.*, 2010, **14**, 269–275.
9 Y. Lu, *Chem.–Eur. J.*, 2002, **8**, 4588–4596.
10 J. Liu, A. K. Brown, X. Meng, D. M. Cropek, J. D. Istok, D. B. Watson and Y. Lu, *Proc. Natl. Acad. Sci. U. S. A.*, 2007, **104**, 2056–2061.
11 Y. Wu, S.-F. Torabi, R. J. Lake, S. Hong, Z. Yu, P. Wu, Z. Yang, K. Nelson, W. Guo, G. T. Pawel, J. Van Stappen, X. Shao, L. M. Mirica and Y. Lu, *Sci. Adv.*, 2023, **9**, eade7622.
12 K. Hwang, Q. Mou, R. J. Lake, M. Xiong, B. Holland and Y. Lu, *Inorg. Chem.*, 2019, **58**, 13696–13708.
13 W. J. Moon, P.-J. J. Huang and J. Liu, *Biochemistry*, 2021, **60**, 1909–1918.
14 B. Cuenoud and J. W. Szostak, *Nature*, 1995, **375**, 611–614.
15 H. Fan, C. E. McGhee, R. J. Lake, Z. Yang, Z. Guo, X.-B. Zhang and Y. Lu, *JACS Au*, 2023, **3**, 1615–1622.
16 W. Ren, P.-J. J. Huang, D. de Rochambeau, W. J. Moon, J. Zhang, M. Lyu, S. Wang, H. Sleiman and J. Liu, *Biosens. Bioelectron.*, 2020, **165**, 112285.
17 J. Liu and Y. Lu, *J. Am. Chem. Soc.*, 2007, **129**, 9838–9839.
18 J. Li, W. Zheng, A. H. Kwon and Y. Lu, *Nucleic Acids Res.*, 2000, **28**, 481–488.
19 P.-J. J. Huang, D. de Rochambeau, H. F. Sleiman and J. Liu, *Angew. Chem., Int. Ed.*, 2020, **59**, 3573–3577.
20 P.-J. J. Huang and J. Liu, *Anal. Chem.*, 2014, **86**, 5999–6005.
21 H. Yu, O. Alkhamis, J. Canoura, Y. Liu and Y. Xiao, *Angew. Chem., Int. Ed.*, 2021, **60**, 16800–16823.
22 S. Qian, D. Chang, S. He and Y. Li, *Anal. Chim. Acta*, 2022, **1196**, 339511.
23 H.-P. Hofmann, S. Limmer, V. Hornung and M. Sprinzl, *RNA*, 1997, **3**, 1289–1300.
24 J. Ciesiolka, J. Gorski and M. Yarus, *RNA*, 1995, **1**, 538–550.
25 R. Nutiu and Y. Li, *Angew. Chem., Int. Ed.*, 2005, **44**, 1061–1065.
26 K. Yang, N. M. Mitchell, S. Banerjee, Z. Cheng, S. Taylor, A. M. Kostic, I. Wong, S. Sajjath, Y. Zhang and J. Stevens, *Science*, 2023, **380**, 942–948.
27 M. Rajendran and A. D. Ellington, *Anal. Bioanal. Chem.*, 2008, **390**, 1067–1075.
28 H. Qu, A. T. Csordas, J. Wang, S. S. Oh, M. S. Eisenstein and H. T. Soh, *ACS Nano*, 2016, **10**, 7558–7565.
29 R. Jahan, A. P. Silwal, S. K. S. Thennakoon, S. P. Arya, R. M. Postema, H. Timilsina, A. M. Reynolds and X. Tan, *Chem. Commun.*, 2023, **59**, 12851–12854.
30 H. Wang, H. Cheng, J. Wang, L. Xu, H. Chen and R. Pei, *Talanta*, 2016, **154**, 498–503.
31 Y. Chen, H. Li, T. Gao, T. Zhang, L. Xu, B. Wang, J. Wang and R. Pei, *Sens. Actuators, B*, 2018, **254**, 214–221.
32 Y. Liu, X. Wang and J. Liu, *Chem. Commun.*, 2024, **60**, 6280–6283.

33 J. Wang, Y. Liu, X. Li, H. Lei and J. Liu, *Chem. Commun.*, 2024, **60**, 14272–14275.
34 C. Bardehle and J. Müller, *Chem.–Eur. J.*, 2025, e202404332.
35 R. K. Sigel and H. Sigel, *Acc. Chem. Res.*, 2010, **43**, 974–984.
36 J. Reedijk, *Proc. Natl. Acad. Sci. U. S. A.*, 2003, **100**, 3611–3616.
37 J. Wang, Y. A. Kaiyum, X. Li, H. Lei, P. E. Johnson and J. Liu, *J. Am. Chem. Soc.*, 2025, **147**, 1831–1839.
38 T.-L. Hwang and A. Shaka, *J. Magn. Reson., Ser. A*, 1995, **112**, 275–279.
39 J. Wang, X. Li, H. Lei and J. Liu, *Anal. Chem.*, 2025, **97**, 9454–9461.
40 O. Alkhamis and Y. Xiao, *J. Am. Chem. Soc.*, 2022, **145**, 194–206.
41 Y. Ding and J. Liu, *J. Am. Chem. Soc.*, 2023, **145**, 7540–7547.
42 Y. Ding, Z. Zhang and J. Liu, *ChemBioChem*, 2024, **25**, e202400570.
43 F. Y. Khusbu, X. Zhou, H. Chen, C. Ma and K. Wang, *Trends Anal. Chem.*, 2018, **109**, 1–18.
44 R. Nutiu and Y. Li, *J. Am. Chem. Soc.*, 2003, **125**, 4771–4778.
45 N. Nakatsuka, K.-A. Yang, J. M. Abendroth, K. M. Cheung, X. Xu, H. Yang, C. Zhao, B. Zhu, Y. S. Rim and Y. Yang, *Science*, 2018, **362**, 319–324.
46 J. Canoura, T. Nguyen, C. Byrd, R. Hill, Y. Liu and Y. Xiao, *Anal. Chem.*, 2024, **96**, 11488–11497.
47 J. Hu and C. J. Easley, *Analyst*, 2011, **136**, 3461–3468.
48 N. Nakatsuka, K.-A. Yang, J. M. Abendroth, K. M. Cheung, X. Xu, H. Yang, C. Zhao, B. Zhu, Y. S. Rim, Y. Yang, P. S. Weiss, M. N. Stojanović and A. M. Andrews, *Science*, 2018, **362**, 319–324.
49 S. Stangherlin, Y. Ding and J. Liu, *Small Methods*, 2024, 2401572.
50 Z. R. Churcher and P. E. Johnson, *Aptamers*, 2020, **4**, 3–9.
51 S. R. Eisen, P. Dauphin-Ducharme and P. E. Johnson, *Q. Rev. Biophys.*, 2024, **57**, e9.
52 R. del Villar-Guerra, J. O. Trent and J. B. Chaires, *Angew. Chem., Int. Ed.*, 2018, **57**, 7171–7175.
53 A. Micsonai, F. Wien, L. Kernya, Y.-H. Lee, Y. Goto, M. Réfrégiers and J. Kardos, *Proc. Natl. Acad. Sci. U. S. A.*, 2015, **112**, E3095–E3103.
54 C. Wang, K. Zhu, P. Shi, X. Ding and S. Zhang, *Chem. Commun.*, 2022, **58**, 4779–4782.
55 N. C. Garbett, P. A. Ragazzon and J. B. Chaires, *Nat. Protoc.*, 2007, **2**, 3166–3172.
56 T. S. Choi and F. A. Tezcan, *Nature*, 2022, **603**, 522–527.
57 P.-J. J. Huang, J. Lin, J. Cao, M. Vazin and J. Liu, *Anal. Chem.*, 2014, **86**, 1816–1821.